

## Using Machine Learning to Screen Non-graphite Carbon Materials Based on Na-Ion Storage Properties

Xiaoxu Liu <sup>a,\*</sup>, Tian Wang <sup>a</sup>, Tianyi Ji <sup>a,\*</sup>, Hui Wang <sup>b</sup>, Hui Liu <sup>a</sup>, Junqi Li <sup>a</sup>, Dongliang Chao <sup>c,\*</sup>

<sup>a</sup> School of Material Science and Engineering, Shaanxi Key Laboratory of Green Preparation and Functionalization for Inorganic Materials, Shaanxi University of Science and Technology, Xi'an, 710021, China.

<sup>b</sup> Division of Physics and Applied Physics School of Physical and Mathematical Sciences, Nanyang Technological University 637371, Singapore.

<sup>c</sup> Laboratory of Advanced Materials, Shanghai Key Laboratory of Molecular Catalysis and Innovative Materials, Fudan University, Shanghai, 200433, China

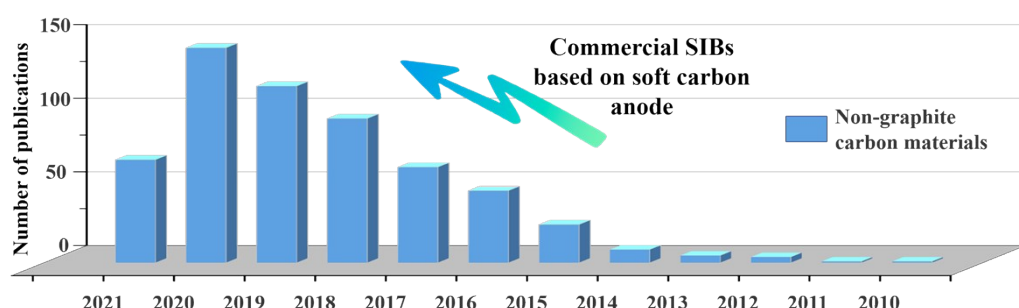


**Fig. S1.** Number of publications on non-graphite carbon materials for SIBs according to Web of Science (as of June 2021). Field Tags and Booleans are TS= (Na ion battery OR Sodium ion battery) AND TS= (hard carbon OR soft carbon OR rGO) NOT TS= (graphite OR graphene OR expanded graphite), where TS=Topic. Then, completely irrelevant articles will be filtered manually.

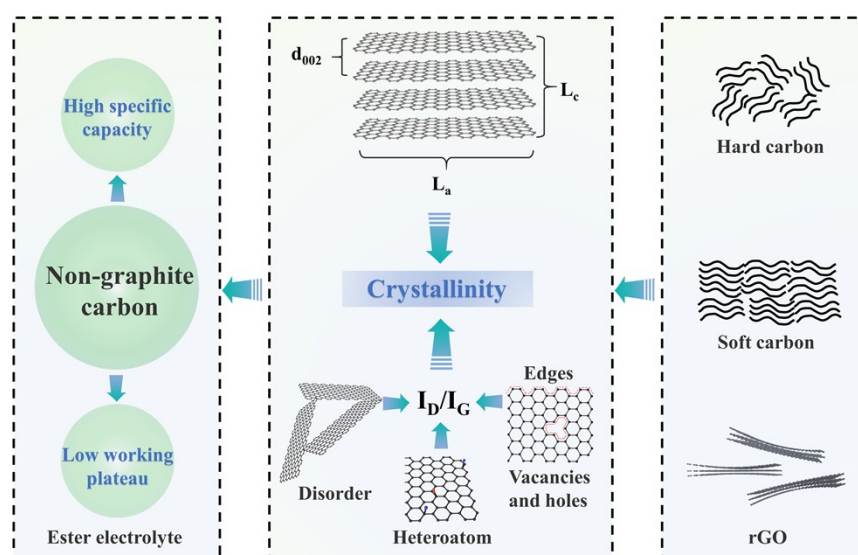


**Fig. S2.** Schematic diagram of key structural parameters, carbon layer structure of main non-graphite carbon materials and their general sodium storage performance.

## Thermodynamic and kinetic analysis

The focus of thermodynamics is whether a reaction can occur and under what conditions. For secondary batteries, ion diffusion barrier and intercalation potential can be calculated by density functional theory or Nernst equation. Therefore, the essential explanation between structural parameters and electrochemical properties should be elaborated from energy potential or chemical potential.

According to the thermodynamics, Qiu et al.<sup>1</sup> calculated the interaction energy function for Na<sup>+</sup> with graphite surface using the Morse form for potential energy:

$$E(r) = E_{ad} (1 - e^{-a(r-r_{eq})})^2 \quad \text{Equation (S1)}$$

The simulation predicts that the interactions between Na<sup>+</sup> and carbon layers depend on the interlayer spacing. For the interlayer spacing between 0.37 and 0.47 nm, the interaction energy between Na<sup>+</sup> and carbon layers has a minimum. The interaction strength increases with interlayer spacing until it reaches 1.38 eV at 0.47 nm. Within this range of 0.37-0.47 nm, Na<sup>+</sup> can truly intercalate into interlayers. Based on the interaction energy between Na<sup>+</sup> and graphitic surfaces, the mechanism for Na<sup>+</sup> incorporation into hard carbon electrode can be analyzed.

Furthermore, Sun et al.<sup>2</sup> confirmed Na<sup>+</sup> can be stored in pseudo-graphitic carbon with an interlayer spacing of 0.36-0.4 nm. The energy of Na<sup>+</sup> intercalation was calculated based on pseudo-graphitic carbon (interlayer spacing is 0.37 nm). The formation energy per carbon atom,  $E_f$ , was calculated by the following equation:

$$E_f[MC_n] = (E[MC_n] - E[C_{n(graphite)}] - E[M_{(metal)}]) / n \quad \text{Equation (S2)}$$

The calculation results identify that the NaC<sub>8</sub> is the most possible Na-GIC structure for pseudo-graphitic carbon and the theoretical capacity is 279 mAh g<sup>-1</sup>.

In addition, the entropy change will be significant in the energy storage process on the basis of Boltzmann's entropy equation:<sup>3, 4</sup>

$$S = k \ln \Omega \quad \text{Equation (S3)}$$

For kinetics, as the carbon layer size reduces and structural disorder increases, the pseudocapacitive behavior is gradually revealed. The contribution of pseudocapacitive adsorption and intercalation to the total capacity can be distinguished by kinetic analysis. At different scan rates, the voltammetry response of the electrode follows the following formula.<sup>5</sup>

$$i = av^b \quad \text{Equation (S4)}$$

$$I(V) = k_1 v + k_2 v^{0.5}$$

Equation (S5)

For instance, Hou et al.<sup>6</sup> prepared self-supporting hard carbon paper at 1300°C. Its plateau region is obviously dominated by diffusion control process, the high-potential slope region is a fast adsorption/desorption process at the surface-active sites including defects.

Similarly, the rate performance related to ion diffusion rate can be studied by kinetic theory and is closely related to specific structural parameters. The ionic diffusion coefficient in electrodes can be determined by solving Fick's second law with the simplified equation:<sup>7</sup>

$$D = \frac{4}{\pi \tau} \left( \frac{m_B V_M}{M_B S} \right)^2 \left( \frac{\Delta E_s}{\Delta E_\tau} \right)^2$$

Equation (S6)

Hence, a thorough survey is dissected from the thermodynamics and kinetics, promoting a more detailed understanding for sodium storage properties of carbon materials. Importantly, this paper expects to further analyze the structure-property data through the previous research on thermodynamics and kinetics, so as to improve the rationality of the data analysis results.

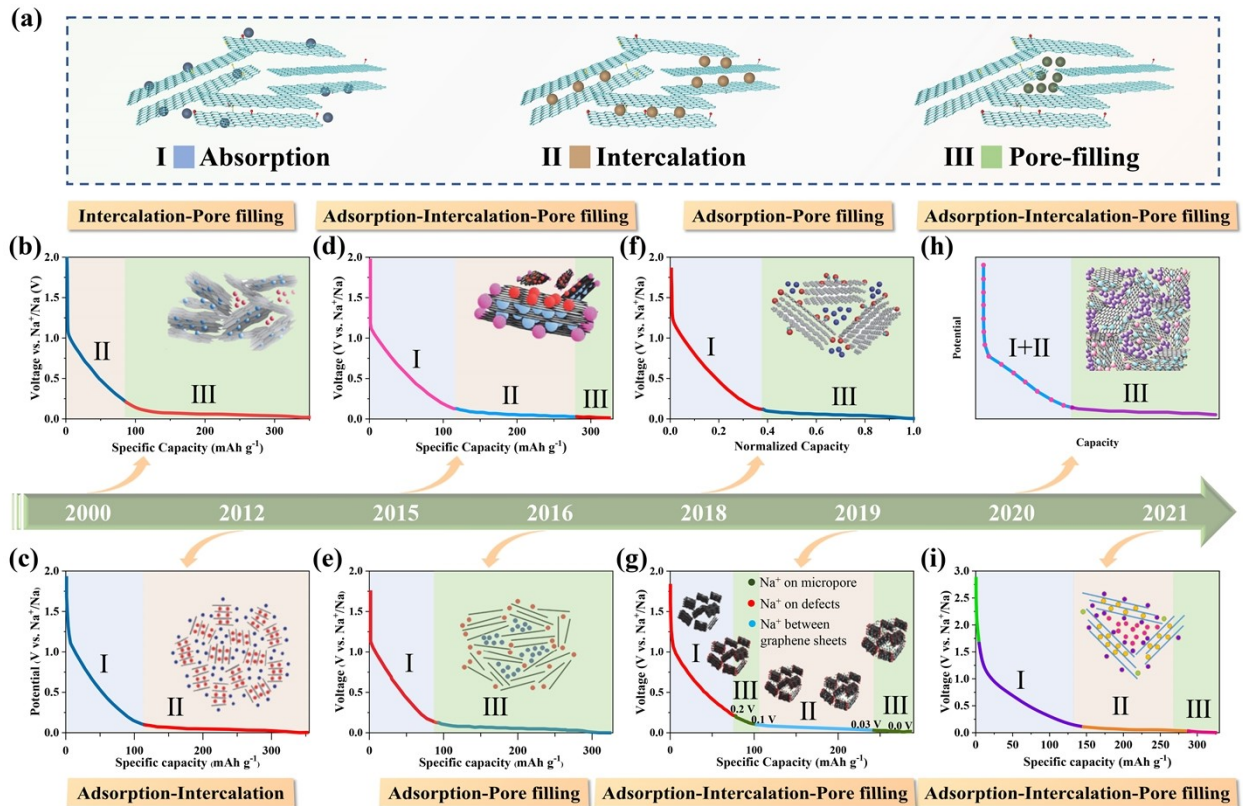


**Fig. S3.** (a) Schematic diagram of  $\text{Na}^+$  distribution corresponding to three sodium storage mechanisms in hard carbon. (b-i) Main research progress in  $\text{Na}^+$  electrochemical intercalation into hard carbon. According to the sodium storage mechanism (I-Absorption, II-Intercalation, III-Pore filling), each discharge curve is divided into different color regions. Fig. (b-i) are reprinted sequentially with permission from ref. 8, Copyright (2015) American Chemical Society; with permission from ref. 1, Copyright (2017) WILEY-VCH; with permission from ref. 8, Copyright (2015) American Chemical Society; with permission from ref. 9, Copyright (2016) WILEY-VCH; with permission from ref. 10, Copyright (2018) WILEY-VCH; with permission from ref. 11, Copyright (2019) Elsevier Ltd.; with permission from ref. 12, Copyright (2020) Royal Society of Chemistry; with permission from ref. 13, Copyright (2021) WILEY-VCH.

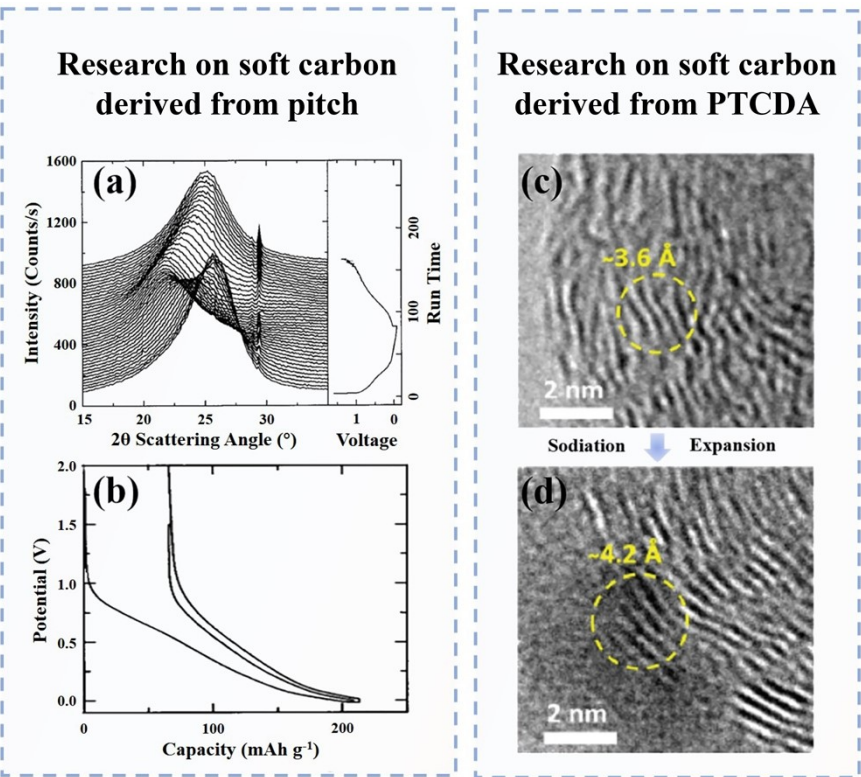


**Fig. S4.** (a, b) Main research progress in  $\text{Na}^+$  electrochemical intercalation into soft carbon and hard-soft carbon composite: (a, b) in situ WAXS spectra and charge-discharge curves of pitch-derived soft carbon. Reproduced with permission from ref. 14, Copyright (2001) IOP Publishing. (c, d) Ex situ HRTEM images of PTCDA-derived soft carbon before and after sodiation to 0.01 V. Reproduced with permission from ref. 15, Copyright (2015), American Chemical Society.

## Section S1

Structure-property database

HTT (°C)	Precursor	d <sub>002</sub> (nm)	L <sub>a</sub> (nm)	L <sub>c</sub> (nm)	I <sub>D</sub> /I <sub>G</sub>	SSA <sub>BET</sub> (m <sup>2</sup> g <sup>-1</sup> )	ICE (%)	Capacity (mAh g <sup>-1</sup> )	Rate factor	Working Plateau (V)
<b>Soft Carbon</b>										
500	NTCDA	0.357	3.11	1.10	0.94	15	46	75.5	0.43	0.82
550	Copolymer	0.383	3.73	0.63	0.97	1106	71	215	0.18	--
700	PTCDA	0.362	--	1.52	--	13.6	62.6	171	0.19	--
700	Pitch	0.351	3.41	1.15	0.87	0.1	66	139	0.15	0.62
800	PTCDA	0.348	2.87	1.56	1.52	471	29	197	0.17	0.69
800	Polymerized acetone	0.369	2.22	0.81	--	467	34	--	0.12	0.73
800	Pitch	0.353	3.85	1.05	1.04	3	71	224	0.12	0.77
800	Pitch	0.349	2.97	1.43	0.91	113	45	135	0.11	0.64
900	PTCDA	0.356	3.69	1.92	--	20	67.6	167	0.30	0.59
900	PTCDA	0.356	3.84	1.41	1.04	14	80	--	0.21	0.91
1100	PTCDA	0.353	4.59	2.43	--	32	60.5	95	0.56	--
1000	HC-SC	0.356	1.66	1.11	0.94	589	57	240 (at 60 mA g <sup>-1</sup> )	0.38	1.43
1000	MP/THF	0.363	2.80	1.27	0.87	59	80	260	0.12	0.63
1300	MP/THF	0.352	3.62	1.74	0.90	89	72	211	0.16	--
1300	Coal	0.371	2.63	0.89	1.02	4.53	79.5	155	0.08	0.58
1400	Pitch/lignin	0.37	3.74	1.17	1.09	1.3	82	245 (at 60 mA g <sup>-1</sup> )	0.16	0.48
1400	Pitch/phenolic resin	0.39	3.27	0.92	1.17	3	88	255 (at 60 mA g <sup>-1</sup> )	0.08	0.51
1500	MP/THF	0.352	4.65	1.97	1.35	32	74	241	0.12	--
1500	Pitch	0.354	2.95	1.75	1.07	119	60	189	0.24	0.64
1600	PTCDA	0.346	5.53	5.27	--	26	47.5	68	0.68	--
<b>Hard Carbon</b>										
600	Peat moss	0.384	2.09	1.08	0.86	369	44	189	0.23	1.02
600	Waste tea bag	0.389	1.61	0.67	0.95	415	58	170	0.33	0.54
700	Pomelo peels	0.371	1.84	0.88	1.04	1272	27	203	0.16	0.79
700	Platanus bark	0.372	1.62	0.76	0.84	602	34	234	0.19	0.87
700	Sepals	0.333	2.33	0.78	0.94	183	70	202	0.14	0.63
800	Banana peel	0.380	4.51	1.58	1.48	217	61	275	0.14	0.77
800	Mangosteen shell	0.367	2.71	1.04	0.97	540	22	50	1.17	0.59
800	Shaddock peel	0.386	1.91	0.81	0.95	25.5	62	216	0.16	0.73
800	Cedarwood bark	0.402	2.25	0.68	0.95	441	44	254	0.23	0.69
900	Peat moss	0.387	2.36	1.08	0.98	271	50	207	0.17	0.78
900	Apricot shell	0.377	1.93	0.67	1.01	27.9	73	282	0.23	0.63
900	Reed straw	0.394	1.95	0.77	1.01	325.3	49	116	0.22	0.62
900	Water caltrop shell	0.385	1.82	0.83	1.01	48.1	76	257	0.14	0.70
900	Bio-oil	0.359	1.70	0.86	1.09	820	56	200	0.23	0.93
950	Sugarcane bagasse	0.369	3.43	0.81	0.97	3	70	232	0.19	0.58

1000	Cellulose	0.375	2.72	0.83	1.05	377	59	235	0.13	0.68
1000	Shaddock peel	0.382	2.25	0.79	0.99	68	63	281	0.12	0.65
1000	Switchgrass	0.368	1.93	1.07	1.16	619	42	199	0.13	0.59
1000	Lotus seedpods	0.377	2.57	0.90	1.08	751.6	45	222	0.11	0.88
1000	Cherry petals	0.404	1.65	0.63	1.02	2	67	235	0.13	0.54
1100	Peat moss	0.374	3.49	0.87	0.99	197	57	281	0.12	0.63
1100	Sucrose	0.412	3.33	0.56	1.30	7	84	151	0.10	0.62
1100	Rice husk	0.395	2.75	0.86	1.01	3	64	332	0.16	0.58
1100	Apricot shell	0.385	2.29	0.72	1.03	56.7	77	328	0.18	0.65
1100	Reed straw	0.394	1.94	0.76	1.02	82	73	260	0.11	0.68
1200	Shaddock peel	0.390	2.60	0.73	1.00	82	67	315	0.08	0.60
1200	Lotus stem	0.371	2.36	0.48	1.06	25.8	69	194	0.19	0.54
1200	Lotus seedpods	0.386	2.69	0.86	1.04	140.7	50	279	0.08	0.81
1200	Tamarind shell	0.392	2.50	0.73	1.02	11.3	70	270	0.08	0.62
1300	Mangosteen shell	0.364	3.33	1.12	1.28	82	74	182	0.20	0.56
1300	Rice husk	0.388	3.08	0.93	0.99	0.3	66	365	0.13	0.59
1300	Reed straw	0.397	2.26	0.75	1.03	36	77	237	0.09	0.62
1300	Walnut shell	0.363	2.83	0.98	1.13	154	46	166	0.16	0.59
1300	Lignin	0.364	3.11	1.26	1.11	10.8	79	283	0.06	0.61
1400	Peat moss	0.373	4.19	0.99	1.03	92	60	240	0.11	0.50
1400	Sucrose	0.403	2.99	0.74	1.05	8	82	206	0.10	0.60
1400	Peat	0.339	3.38	2.19	0.98	6	80	303	0.08	0.51
1400	Shaddock peel	0.383	3.27	0.84	1.69	39	69	223	0.09	0.58
1500	Mangosteen shell	0.359	3.87	1.17	1.40	8.96	83	134	0.14	0.55
1500	RF resin	0.390	2.88	0.78	1.07	450	57	69	0.13	0.73
1500	Reed straw	0.381	2.99	0.90	1.05	23.9	79	210	0.09	0.62
1500	Water caltrop shell	0.376	3.25	0.95	1.01	7.4	86	236	0.11	0.56
1600	Sucrose	0.395	3.95	0.88	1.17	5	85	275	0.09	0.60
1600	Cellulose	0.386	4.03	0.79	1.16	2	81	51	0.12	0.52
1600	Lotus stem	0.350	2.73	1.21	1.24	23.7	56	240	0.08	0.49
1600	Corn straw piths	0.360	2.19	0.72	0.93	10	55	180	0.15	0.76
2050	Switchgrass	0.352	3.07	1.48	1.05	23	64	204	0.21	0.56

References were cited for all data.

## Section S2

In this work, 5-fold cross validation is applied to process raw data. The five structural parameters of  $d_{002}$ ,  $L_a$ ,  $L_c$ ,  $I_D/I_G$ , SSA are independent variables and serve as input data to the model. ICE, Capacity and Rate factor as the dependent variable are the output of the model, which is the prediction target.

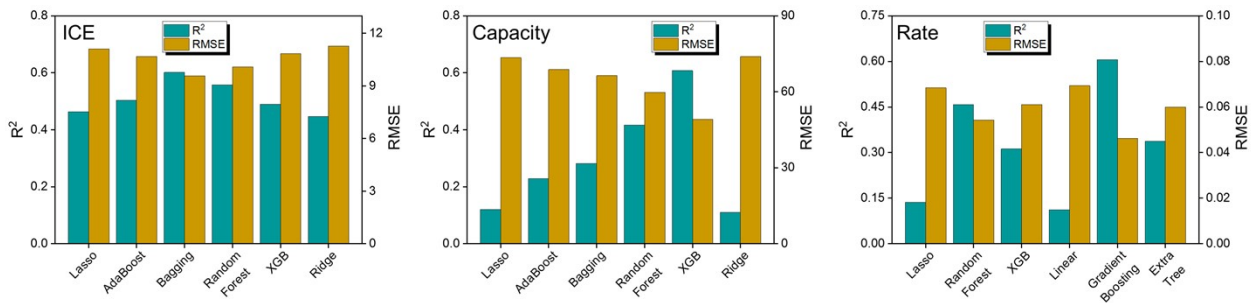


**Fig. S5.** The values of  $R^2$  and RMSE of different machine learning models for ICE, Capacity and Rate performance. The model with the highest  $R^2$  and lowest RMSE is selected for further analysis in body paragraphs (Bagging Regressor for ICE, XGB Regressor for Capacity and Gradient Boosting Regressor for Rate).

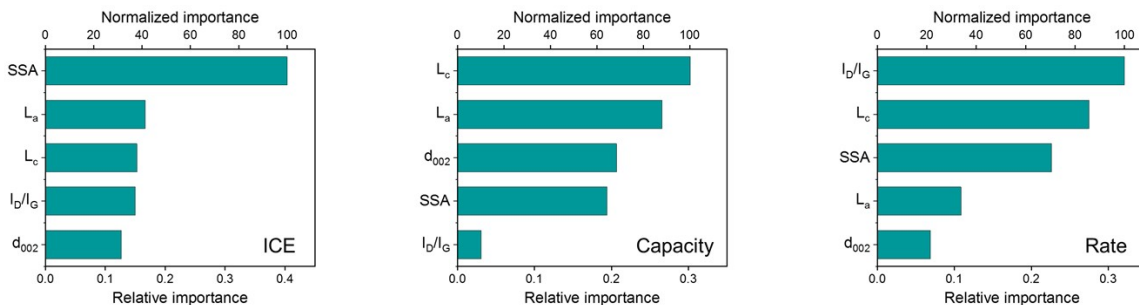


**Fig. S6.** Feature importance analysis for ICE, Capacity and Rate performance based on Neural Network.

Table S1 Structural parameters and sodium storage performance of rGO

Materials	Electrolyte	$d_{002}$ (nm)	$I_D/I_G$	ICE (%)	Capacity (mAh g <sup>-1</sup> )	Rate factor	Working Plateau (V)
rGO <sup>16</sup>	1M NaClO <sub>4</sub> in PC	0.335	1.23	20	214	0.13	0.47
rGO <sup>17</sup>	1M NaPF <sub>6</sub> in EC-DMC	0.364	0.97	24	117	0.38	0.32
rGO <sup>18</sup>	1M NaPF <sub>6</sub> in EC-DEC	0.361	--	80	240	0.09	0.96
Fe-rGO <sup>19</sup>	1M NaClO <sub>4</sub> in EC-PC-FEC	0.394	1.07	26	134	0.24	0.89
Sn-rGO <sup>19</sup>	1M NaClO <sub>4</sub> in EC-PC-FEC	0.379	1.09	32	145	0.17	1.14
rGO <sup>20</sup>	1M NaClO <sub>4</sub> in EC-DMC-FEC	0.408	1.13	--	251	0.15	1.40
H-rGO <sup>20</sup>	1M NaClO <sub>4</sub> in EC-DMC-FEC	0.415	1.05	52.7	364	0.13	1.39

Table S2 Structural parameters and sodium storage performance of graphite-like carbon materials

Materials	Electrolyte	$d_{002}$ (nm)	$I_D/I_G$	ICE (%)	Capacity (mAh g <sup>-1</sup> )	Rate factor	Working Plateau (V)
SFG-44 Graphite <sup>21</sup>	1 M NaCF <sub>3</sub> SO <sub>3</sub> in DEGDME	0.336	--	88.2	82	1.20	0.96
Natural graphite <sup>22</sup>	1 M NaPF <sub>6</sub> in DME	0.336	0.06	56.7	145	0.55	0.48
Natural graphite <sup>22</sup>	1 M NaPF <sub>6</sub> in DEGDME	0.336	0.06	50.9	155	0.83	0.50
Natural graphite <sup>22</sup>	1 M NaPF <sub>6</sub> in TEGDME	0.336	0.06	57.5	141	0.47	0.57
Natural graphite <sup>23</sup>	1 M NaCF <sub>3</sub> SO <sub>3</sub> in TEGDME	0.336	0.18	87.9	112	6.83	0.87
Natural graphite <sup>24</sup>	1 M NaClO <sub>4</sub> in TEGDME	--	--	79.7	98	4.04	0.82
Graphite <sup>25</sup>	1 M NaCF <sub>3</sub> SO <sub>3</sub> in DEGDME	--	--	85.8	102	1.72	0.80
Graphite <sup>26</sup>	1 M NaPF <sub>6</sub> in DEGDME	--	0.12	64.9	143	0.67	0.82
Few-Layered Graphene <sup>27</sup>	1 M NaPF <sub>6</sub> in DEGDME	--	0.02	58.8	192	0.91	0.80
Expanded Graphite <sup>28</sup>	1 M NaCF <sub>3</sub> SO <sub>3</sub> in DEGDME	0.339	0.03	61.9	120	--	0.54

## Section S3

By collating the existing structure data, the Table S3 shows the minimum and maximum values for each structural variable. The values were produced at specified intervals to avoid bias and errors caused by a change in the method of measurement (except for  $SSA_{BET}$ , which is a random number). The virtual structure data set was then obtained by simply permutation and combination.

Table S3 the basic data of construction for structure data set

	$d_{002}$ [nm]	$L_a$ [nm]	$L_c$ [nm]	$I_D/I_G$	$SSA_{BET}$ [m <sup>2</sup> g <sup>-1</sup> ]
Minimum <sup>a</sup>	0.335	0.5	0.3	0.23	2
Maximum <sup>a</sup>	0.425	5	2.8	1.63	1272
Methods <sup>b</sup>	$\Delta=0.015$	$\Delta=0.5$	$\Delta=0.5$	$\Delta=0.2$	random
Results <sup>c</sup>	0.335	0.5	0.3	0.23	2
	0.35	1	0.8	0.43	160
	0.365	1.5	1.3	0.63	325
	0.38	2	1.8	0.83	587
	0.395	2.5	2.3	1.03	850
	0.41	3	2.8	1.23	1272
	0.425	3.5		1.43	
		4		1.63	
		4.5			
		5			

<sup>a</sup> from the range of existing research data. <sup>b</sup>  $\Delta$  represents difference value. <sup>c</sup> the structure data set is obtained by permutation and combination.

## References

1. S. Qiu, L. Xiao, M. L. Sushko, K. S. Han, Y. Shao, M. Yan, X. Liang, L. Mai, J. Feng and Y. Cao, *Adv. Energy Mater.*, 2017, **7**, 1700403.
2. N. Sun, Z. Guan, Y. Liu, Y. Cao, Q. Zhu, H. Liu, Z. Wang, P. Zhang and B. Xu, *Adv. Energy Mater.*, 2019, **9**, 1901351.
3. J. Sun, G. Zheng, H.-W. Lee, N. Liu, H. Wang, H. Yao, W. Yang and Y. Cui, *Nano Lett.*, 2014, **14**, 4573-4580.
4. J. Sun, H.-W. Lee, M. Pasta, H. Yuan, G. Zheng, Y. Sun, Y. Li and Y. Cui, *Nat. Nanotechnol.*, 2015, **10**, 980-985.
5. P. Simon, Y. Gogotsi and B. Dunn, *Science*, 2014, **343**, 1210-1211.
6. B.-H. Hou, Y.-Y. Wang, Q.-L. Ning, W.-H. Li, X.-T. Xi, X. Yang, H.-J. Liang, X. Feng and X.-L. Wu, *Adv. Mater.*, 2019, **31**, 1903125.
7. Z. Jian, Z. Xing, C. Bommier, Z. Li and X. Ji, *Adv. Energy Mater.*, 2016, **6**, 1501874.
8. C. Bommier, T. W. Surta, M. Dolgos and X. Ji, *Nano Lett.*, 2015, **15**, 5888-5892.
9. Y. Li, Y.-S. Hu, M.-M. Titirici, L. Chen and X. Huang, *Adv. Energy Mater.*, 2016, **6**, 1600659.
10. P. Bai, Y. He, X. Zou, X. Zhao, P. Xiong and Y. Xu, *Adv. Energy Mater.*, 2018, **8**, 1703217.
11. S. Alvin, D. Yoon, C. Chandra, H. S. Cahyadi, J.-H. Park, W. Chang, K. Y. Chung and J. Kim, *Carbon*, 2019, **145**, 67-81.
12. H. Au, H. Alptekin, A. C. S. Jensen, E. Olsson, C. A. O'Keefe, T. Smith, M. Crespo-Ribadeneyra, T. F. Headen, C. P. Grey, Q. Cai, A. J. Drew and M.-M. Titirici, *Energy Environ. Sci.*, 2020, **13**, 3469-3479.
13. Z. Wang, X. Feng, Y. Bai, H. Yang, R. Dong, X. Wang, H. Xu, Q. Wang, H. Li, H. Gao and C. Wu, *Adv. Energy Mater.*, 2021, **11**, 2003854.
14. D. A. Stevens and J. R. Dahn, *J. Electrochem. Soc.*, 2001, **148**, A803.
15. W. Luo, Z. Jian, Z. Xing, W. Wang, C. Bommier, M. M. Lerner and X. Ji, *ACS Central Sci.*, 2015, **1**, 516-522.
16. Y.-X. Wang, S.-L. Chou, H.-K. Liu and S.-X. Dou, *Carbon*, 2013, **57**, 202-208.
17. L. David and G. Singh, *J. Phys. Chem. C*, 2014, **118**, 28401-28408.
18. J. Wan, F. Shen, W. Luo, L. Zhou, J. Dai, X. Han, W. Bao, Y. Xu, J. Panagiotopoulos, X. Fan, D. Urban, A. Nie, R. Shahbazian-Yassar and L. Hu, *Chem. Mater.*, 2016, **28**, 6528-6535.
19. N. A. Kumar, R. R. Gaddam, S. R. Varanasi, D. Yang, S. K. Bhatia and X. S. Zhao, *Electrochim. Acta*, 2016, **214**, 319-325.
20. J. Zhao, Y.-Z. Zhang, F. Zhang, H. Liang, F. Ming, H. N. Alshareef and Z. Gao, *Adv. Energy Mater.*, 2019, **9**, 1803215.
21. B. Jache and P. Adelhelm, *Angew. Chem., Int. Ed.*, 2014, **53**, 10169-10173.
22. H. Kim, J. Hong, Y.-U. Park, J. Kim, I. Hwang and K. Kang, *Adv. Funct. Mater.*, 2015, **25**, 534-541.
23. Z. Zhu, F. Cheng, Z. Hu, Z. Niu and J. Chen, *J. Power Sources*, 2015, **293**, 626-634.
24. I. Hasa, X. Dou, D. Buchholz, Y. Shao-Horn, J. Hassoun, S. Passerini and B. Scrosati, *J. Power Sources*, 2016, **310**, 26-31.
25. H. Kim, G. Yoon, K. Lim and K. Kang, *Chem. Commun.*, 2016, **52**, 12618-12621.

26. Z. Wang, H. Yang, Y. Liu, Y. Bai, G. Chen, Y. Li, X. Wang, H. Xu, C. Wu and J. Lu, *Small*, 2020, **16**, 2003268.
27. A. P. Cohn, K. Share, R. Carter, L. Oakes and C. L. Pint, *Nano Lett.*, 2016, **16**, 543-548.
28. M. Cabello, X. Bai, T. Chyrka, G. F. Ortiz, P. Lavela, R. Alcántara and J. L. Tirado, *J. Electrochem. Soc.*, 2017, **164**, A3804-A3813.